Dynamics of the $C_2H_2^+ + ND_3$ Reaction: A Vibrational-Mode-Selective Scattering Study

Jun Qian, Hungshin Fu, and Scott L. Anderson*

Department of Chemistry, University of Utah, Salt Lake City, Utah 84112

Received: February 26, 1997; In Final Form: April 14, 1997[⊗]

The $C_2H_2^+ + ND_3$ reaction has been studied using mode-selective preparation of the $C_2H_2^+$ reactant in conjunction with measurements of the product ion recoil velocity distributions. The only product channels observed over a collision energy range from 0.1 to 5 eV (CM) are ND_3^+, ND_3H^+, and ND_2H^+. No evidence for the formation of covalently bound intermediates is found, despite the existence of several strongly bound isomers of $C_2H_5N^+$. Also not observed is H atom abstraction. The absence of these channels is surprising in light of their importance in the energetically similar $C_2H_2^+ + CH_4$ system. The ND_3^+ charge-transfer reaction is found to proceed at low collision energies via a weakly bound $[C_2H_2{:}ND_3]^+$ intermediate with lifetime around 1 ps. At high energies, charge transfer occurs mostly by long-range electron hopping. Proton transfer is direct at all energies, though the time scale of the collisions approaches 300 fs at low energies. Vibrational effects are mode-specific and change with collision energy and product channel. A collision energy and vibrational-mode-dependent reaction mechanism is proposed.

I. Introduction

We have been studying the reaction dynamics of small polyatomic cations,[1−11] choosing systems that show many of the complexities of larger systems but that are still simple enough to be probed in detail, experimentally and theoretically. A combination of several tools is needed to work out the dynamics of these reactions. We measure the integral cross sections for all the observed products as a function of collision energy and vibrational state of the reactant cation. Vibrational-mode specificity is a sign that some transition state (TS), *early in the collision*, is controlling the reactivity and that particular types of motion or reactant distortion can enhance or inhibit passage through the TS. The TS must be early, before the intimate collision can scramble the initially prepared vibrational mode. We measure the velocity distributions for all the product ions, and this provides several types of information. The degree of forward−backward symmetry provides insight into the importance of complex-mediated vs direct reaction mechanisms. For direct mechanisms, the distributions allow further classification as stripping-, rebound-, or glancing-type collisions. Finally, by extracting the recoil energy distributions from the velocity information, we can determine energy partitioning and also look for the effects of exit channel barriers. Of course, we also take advantage of standard techniques such as isotope labeling, etc.

The $C_2H_2^+ + NH_3$ system was chosen because it is isoelectronic with, and energetically similar to, the $C_2H_2^+ + CH_4$ system, where we previously have found interesting dynamics, including the largest vibrational-mode effects observed to data.[4,5] (The fact that the two systems are isoelectronic influences what electronic surfaces are likely to be important and thus has some relevance to a nonadiabatic reaction.) The potential surface for the $C_2H_2^+/CH_4$ system has a number of deep wells corresponding to various isomeric forms of covalently bound $C_3H_6^+$. At low collision energies, the dominant reactions correspond to H, H_2, or CH_3 elimination from a long-lived $C_3H_6^+$ complex, and when deuterium labels are used, the product distribution appears to be statistical. Formation of the long-lived complex is only ∼50% efficient at low energies and is inhibited by collision energy and acetylene CC-stretch excitation but enhanced by excitation of the $C_2H_2^+$ bend.

In addition to these complex-mediated reaction channels, H atom abstraction is observed, and this becomes the dominant reaction at collision energies above ∼1 eV. Both isotope labeling and recoil velocity measurements show that the mechanism is direct, switching from a short-lived (∼1-ps) complex at low energies to a stripping mechanism at high energies. This product channel is ∼150 meV endoergic, and as might be expected, reaction is enhanced by collision energy in the threshold energy range. Acetylene CC-stretch excitation has little effect, however, and bend excitation produces a large enhancement that persists well past the threshold energy range.

The strong bending enhancements were taken as evidence that there must be at least two *early* bent transition states, controlling the direct and complex-mediated reaction channels. Subsequently, Klippenstein[12] reported an *ab initio* study of the important stationary points on the $C_2H_2^+/CH_4$ surface. This revealed three separate forms of weakly bound $C_2H_2^+{:}CH_4$ complexes with transition states, leading either to $C_2H_3^+$ or $C_3H_6^+$ complexes. He also reported transition-state theory calculations of vibrational effects and found qualitative agreement with our results.

A simple potential energy diagram for the $C_2H_2^+/NH_3$ system is shown in Figure 1. Only product species and covalently bound intermediates are shown, though analogy with the methane system suggests that weakly bound $[C_2H_2{:}NH_3]^+$ minima may also exist in the entrance channel. Energetics for the various local minima were calculated using data from the compilation of Lias et al.[13] There are many points of similarity with the energetics for $C_2H_2^+/CH_4$. There are a number of covalently bound $C_2H_5N^+$ species that could serve as intermediates in a complex-mediated mechanism. These species are actually more stable than the analogous $C_3H_6^+$ complexes, and lifetimes[14] in the 100-ps to 10-ns range would be expected for our collision energies. Just as in the methane system, there are exoergic channels corresponding to H and H_2 elimination from the $C_2H_5N^+$ complex, and the reaction analogous to CH_3 elimination (i.e., NH_2 elimination) would give the H atom abstraction products. H atom abstraction is about 60% more

* Author to whom correspondence should be addressed.
[⊗] Abstract published in *Advance ACS Abstracts,* July 15, 1997.

S1089-5639(97)00722-6 CCC: $14.00

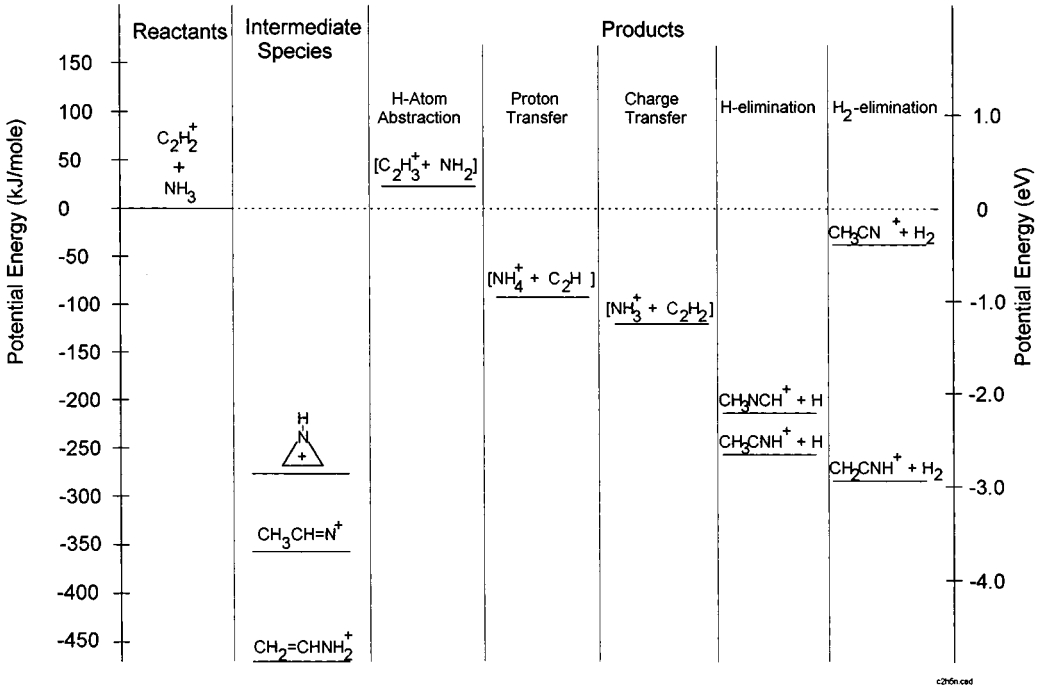

Figure 1. Potential energy diagram, showing reactants, potential products, and covalently bound intermediates.

endoergic for NH_3 than CH_4, but note that this is still small compared to the energy available except at our lowest collision energies.

There are two exoergic channels for $C_2H_2^+ + NH_3$ not seen in the methane case. The proton affinity of NH_3 (8.85 eV[15]) is large enough to make proton transfer exoergic, while for CH_4 (PA = 5.7 eV) this reaction is endoergic. For methane, PT is not observed over the 0−5-eV collision energy range; however, it does occur for reaction of $C_2H_2^+$ that has been vibrationally excited near its dissociation limit.[16] Similarly, charge transfer from $C_2H_2^+$ to NH_3 is 1.24 eV exoergic, while for CH_4 it is endoergic by 1.1 eV. Perhaps more important is the difference in vertical ionization energies (IE's), since both CH_4 and NH_3 undergo large geometry changes upon ionization. For NH_3, the vertical IE[17] is ∼0.8 higher than the adiabatic IE; thus, vertical charge transfer is ∼0.4 eV exoergic. For CH_4, ionization only begins to have reasonable Franck−Condon factors about ∼0.8 eV above the adiabatic IE; thus, the vertical charge-transfer process is >2 eV endoergic, and this channel is not observed.

From the comparison of the two systems, we expected similar dynamics, though with product branching modified by the presence of the two additional exoergic channels. We have not found in the literature any studies of the $C_2H_2^+ + NH_3$ reaction except in a compilation of 300 K ICR measurements by Huntress.[18] He reported observing only proton-transfer and charge-transfer products, with a 0.31:069 branching ratio. We would expect similar product branching at the lowest energies in our experiments but possibly quite different chemistry as the increasing collision opens endoergic channels and channels with barriers.

II. Experimental Details

A. Instrumentation and Operating Conditions. The guided ion beam tandem mass spectrometer used in these experiments, along with our operating, calibration, and data analysis procedures, has been described previously.[5] The MPI routes that we use to prepare state-selected reactants have been discussed in detail.[19,20] (3 + 1) MPI via the $G^1\Pi_u$ origin, 2_0^1, and 2_0^2 bands results in production of $C_2H_2^+$ in the ground, $\nu_2 = 1$, and $\nu_2 = 2$ levels, with high purity. The same ion levels can also be prepared by (2 + 1) MPI via a ν_2 progression in the $^1\Delta_g$ state. In addition to the preparation of ions with excitation in the Franck−Condon-allowed ν_2 (C−C-stretch) mode, ionization via mixed intermediate levels can produce ions with $2\nu_{bend}$ excitation. From our photoelectron spectra, it was not possible to identify which bend was excited, and we tentatively picked ν_5 (cis bend) based on rotational contour symmetry. While we cannot rule out the trans bend, the effects on reactivity in the reaction of $C_2H_2^+$ with methane[4,12] and with OCS[10] support the cis-bend assignment.

State-selected ions are produced in the center of a quadrupole in guide by MPI of a pulsed, differentially pumped supersonic beam. A combination of focusing in the ion guide and time-of-flight (TOF) gating is used to reject fragment ions produced in MPI and narrow the kinetic energy distribution. The mass-selected reactant ions are then injected into a short segment of octapole ion guide where they pass through a scattering cell containing ND_3 at a pressure of 8×10^{-5} Torr, as measured by a capacitance manometer (MKS Baratron Type 390HA-001). ND_3 (Cambridge Isotope Labs, >99%) is used to distinguish atom/proton-transfer processes and atom scrambling. Product ions and the remaining reactant ions are collected by the octapole, guided through a second, longer octapole segment, mass analyzed, and counted by a Daly detector. Reactant and product ion velocity distributions are measured using time of flight (TOF).

Integral cross sections were measured for each reactant vibrational state at collision energies ranging from 0.1 to 5 eV (center of mass). The data for all vibrational levels were taken consecutively to ensure reliability in the comparisons, and the entire set of experiments was repeated several times. For integral cross sections, the final electrode injecting ions into the octapole guide is set and/or pulsed so that product ions backscattered in the LAB frame are reflected and thus guided to the final mass filter.

The quadrupole and octapole ion guides are driven at 3.8 and 6.1 MHZ, respectively. Each is powered by a homemade high-power oscillator, directly coupled to the guide. The operating frequency can be adjusted over a wide range, and the rf amplitude can be precisely controlled, either manually, or by

computer. Amplitude control is important both for energy selection in the quadrupole and for measuring radial velocities (see below) in the octapole. In addition of the dc potential applied to set the ion energy, the rf supplies allow a differential dc bias to be applied for effective potential calibration. Finally, the rf can be turned off and ramped up under control of a TTL pulse to allow rejection of unwanted ions.

B. Correction for Secondary Reactions. Measurements were made for ND_3 scattering gas pressures ranging from 3×10^{-5} to 1.5×10^{-4} Torr to assess multiple collision effects. It appears that our typical operating range (8×10^{-5} Torr) is low enough to make multiple collisions of the primary ions insignificant. Another problem is important, however. As shown below, many of the product ions are backscattered in the CM frame, corresponding to low LAB frame velocities. These slow ions have a high probability for secondary reactions with the ND_3 in the scattering cell, e.g.,

$$C_2H_2^+ + ND_3\ (+ND_3) \rightarrow ND_3^+ + C_2H_2 + ND_3 \rightarrow ND_4^+ + C_2H_2 + ND_2 \quad (1a)$$

$$C_2H_2^+ + ND_3\ (+ND_3) \rightarrow ND_2H^+ + C_2HD + ND_3 \rightarrow ND_4^+ + C_2HD + NDH \quad (1b)$$

$$C_2H_2^+ + ND_3\ (+ND_3) \rightarrow ND_2H^+ + C_2HD + ND_3 \rightarrow ND_3H^+ + C_2HD + ND_2 \quad (1c)$$

where the second step in each sequence is a isotopic variant on the reaction $NH_3^+ + NH_3 \rightarrow NH_4^+ + NH_2$, which occurs near the collision rate for low-energy ions.[21]

The practical lower limit on the ND_3 pressure is set by our need for a reasonable (>1%) probability for the primary $C_2H_2^+ + ND_3$ reactions, and this is not sufficient to completely eliminate the secondary reactions. What we have done is to try to identify which primary products contribute to the secondary product ion signal. This is done by comparing apparent cross sections taken at high, normal, and low ND_3 scattering gas pressures. There are four masses with significant ion signal. Mass 19 corresponds to ND_2H^+, mass 20 is ND_3^+ and possibly $ND_2H_2^+$, mass 21 is ND_3H^+, and mass 22 is ND_4^+.

A 3×10^{-5} Torr, the apparent ND_4^+ cross section at low collision energies is ~3 Å^2, increasing to ~16 Å^2 as the pressure is raised to 1.5×10^{-4} Torr. Over this same pressure range, the mass 20 apparent cross section drops from 35.5 to 23 Å^2. The fact that these two cross sections have almost equal but opposite effects indicates that the bulk of the ND_4^+ signal comes from $ND_3^+ \rightarrow ND_4^+$ (reaction 1a). This is expected since charge transfer, especially if resonant channels exist, may yield ions that are very slow in the LAB frame. These ions therefore spend a long time in the ND_3-filled scattering cell and react with high probability.

The ND_2H^+ product has a much weaker pressure dependence, indicating that this "charge-transfer" isotopomer is less likely to undergo secondary reaction than the main ND_3^+ product. Since the intrinsic reactivity of the two isotopomers must be similar, the implication is that there are fewer very slow (and thus reactive) ND_2H^+ product ions. This is to be expected since the atom scrambling needed to produce ND_2H^+ must result in some momentum transfer.

The other question is to what extent proton exchange might convert the ND_3H^+ primary product to ND_4^+:

$$C_2H_2^+ + ND_3\ (+ND_3) \rightarrow ND_3H^+ + C_2H + ND_3 \rightarrow ND_4^+ + C_2H + ND_2H \quad (2a)$$

We find that the ND_3H^+ apparent cross section increases as the pressure is lowered, but the effect is only at the 5% level. Proton exchange is reported[22] to be highly efficient at low energies, but for this case, we expect that momentum transfer in the initial reaction will reduce the chance of producing very slow ND_3H^+ that would undergo efficient secondary reaction.

In presenting the data below, we have simply added the ND_4^+ signal to the mass 20 signal before calculating the cross sections, i.e., assumed that all ND_4^+ came from reaction 1a. This probably overstates the magnitude of the mass 20 cross section by about 1−2% and may underestimate the cross sections for ND_2H^+ and ND_3H^+ by 3−6%. In the more important question of comparing cross sections from the reaction of different $C_2H_2^+$ vibrational states, we believe that the error introduced by this assumption is negligible—none of our velocity distribution measurements show a significant dependence on the $C_2H_2^+$ state; thus, the secondary reaction probabilities should also be state independent.

C. Product Ion Velocity Distributions and Analysis. In addition to the integral cross sections, we also measured the recoil velocity distributions for all the product ions, for a range of collision energies. Some measurements were made for all the $C_2H_2^+$ reactant vibrational states, but since the effects on the recoil energies are insignificant, the bulk of the measurements focus on the reaction of ground-state $C_2H_2^+$.

Two types of measurements were made. We attempted to determine true doubly-differential cross sections using the TOF/variable guiding field approach developed by Gerlich.[23] The idea is simple and takes advantage of the cylindrical symmetry of the experiment. In this symmetry, any product recoil velocity vector can be broken down into components parallel and perpendicular to the octapole axis—v_{axial} and v_{radial}. (The velocity distribution is two-dimensional because the experiment is azimuthally symmetric.) The distribution of v_{axial} can be measured by recording the TOF distribution of the product ions, and by measuring v_{axial} distributions for a range of octapole rf amplitudes, it is possible to extract the full two-dimensional velocity distribution. For this system, the primary ion/product ion mass ratio results in poor v_{radial} resolution. The analysis below is based on v_{axial} distributions measured at high octapole rf amplitude, i.e., the projections of the full velocity distributions on the octapole axis.

Because, on average, v_{rel} (the relative velocity in the collisions) is coaxial with the ion guide, much of the important dynamical insight, such propensity to forward/backward scattering, can be obtained directly from inspection of the v_{axial} distributions. Quantitative analysis requires fitting the experimental data, as follows.[5,10] A trial recoil velocity distribution is assumed and then fed into a Monte Carlo simulation of the experiment, accounting for broadening factors such as the ion beam and target velocity distributions, target rotational energy distribution, etc. The simulation gives v_{axial} and v_{radial} distributions and also correctly averaged values for v_{rel}, E_{col}, V_{CM}, and E_{avail}, respectively, the relative velocity, and collision energy, the LAB velocity of the center of mass, and the total energy available to the products. The trial velocity distribution is then adjusted until the resulting v_{axial}/v_{radial} distributions are in agreement with experiment. The accuracy of the calibration/TOF-to-velocity inversion/simulation process is tested by using velocity distributions measured for $C_3H_5^+$ produced in reaction of $C_2H_2^+$ with CH_4. As required by kinematics and the reaction mechanism,[5] the result is a sharp peak symmetric about V_{CM}.

Since the experiment primarily gives axial projections of the full product velocity distributions, there is a uniqueness problem in fitting trial two-dimensional distributions to the data. The best we can do is to use a physically reasonable model for the

dynamics to generate trial velocity distributions. The resulting fits are therefore reasonable but necessarily somewhat model-dependent. The trial velocity distributions are based on the "osculating complex" model of Fisk et al.[24] It is assumed that the colliding reactants form a complex with lifetime $\tau_{complex}$ and rotational period τ_{rot}. In addition, it is assumed that the products recoil in some direction (θ_{peak}) relative to the rotating frame of the complex. In this model,$\tau_{rot}/\tau_{complex} < 1$ corresponds to a collision where the complex makes at least a full rotation and therefore loses all directional "memory" prior to product recoil. This results in a velocity distribution that is isotropic in the scattering plane. Conversely, a large value for $\tau_{rot}/\tau_{complex}$ corresponds to a short, direct collision where products will be scattered close to θ_{peak}.

The clock for the dynamics is the complex rotational period, τ_{rot}. Classically, this can be estimated by $\tau_{rot} = 2I_{complex}/\hbar l$, where $I_{complex}$ is the moment of inertia and $l = \mu v_{rel} b$ is the orbital angular momentum of the reactants (μ = reduced mass, b = impact parameter). For reasonable values of $I_{complex}$ and l (estimated from the magnitude of the cross section), the rotational period works out to about 1 ps. Within the uncertainties associated with l and $I_{complex}$, this 1-ps period is approximately independent of the collision energy (E_{col}), because the changes in v_{rel} ($=[2E_{col}/\mu]^{1/2}$) are offset by changes in the range of impact parameters leading to reaction (i.e., $\sigma_{tot} \approx \pi b_{max}^2$ varies from ~140 to ~15 Å^2 as E_{col} varies from 0.1 to 5 eV).

To complete the trial velocity distribution, we use the following recoil *energy* distribution to specify the recoil speeds:

$$P(E_{recoil}) = \exp\left(-\left(\frac{f_{width}(E_{recoil} - f_{peak}E_{avail})}{E_{avail}}\right]^2\right)$$

This is a Gaussian in energy, with a peak energy of $f_{peak}E_{avail}$ and a width proprotional to E_{avail}/f_{width}. In the simulation program, the high-energy tail of the distribution is truncated on a collision-by-collision basis to ensure that the total energy is conserved. Other functions that include angle-speed coupling have been tried, but this gives an acceptable fit with a minimum of parameters.

The nice thing about this model is that it allows description of a wide variety of recoil velocity distributions with just four parameters (f_{peak}, f_{width}, θ_{peak}, and $\tau_{rot}/\tau_{complex}$), all of which are physically meaningful. Since much of the dynamical insight comes from comparison of velocity distributions for different products at different energies, we try to fit the data using parameter sets that are as consistent as possible (e.g., f_{peak} parameters that vary smoothly with energy). Further details and tests of how well the data constrain the resulting dynamics can be found in our paper on the $C_2H_2^+ + CH_4$ system.[5]

III. Results

The integral cross sections for all observed product ions are plotted as a function of collision energy and $C_2H_5^+$ vibrational state in Figure 2. To our surprise, only three of the many possible product channels have significant intensity. This was expected for low collision energies, since the thermal energy measurement of Huntress[18] had found only charge-transfer (CT) and proton-transfer (PT) products. (Huntress studied $C_2H_2^+ + NH_3$ and was unable to distinguish between CT with and without H atom exchange.)

All three channels have similar collision energy dependence, being strongly inhibited by increasing energy. For reference, the total cross section for the reaction of ground state $C_2H_2^+$ is plotted as a heavy dashed line in the center frame of the figure. Also plotted in the center frame is an estimate of the collision cross section, taken to be the ion−dipole capture cross section[25]

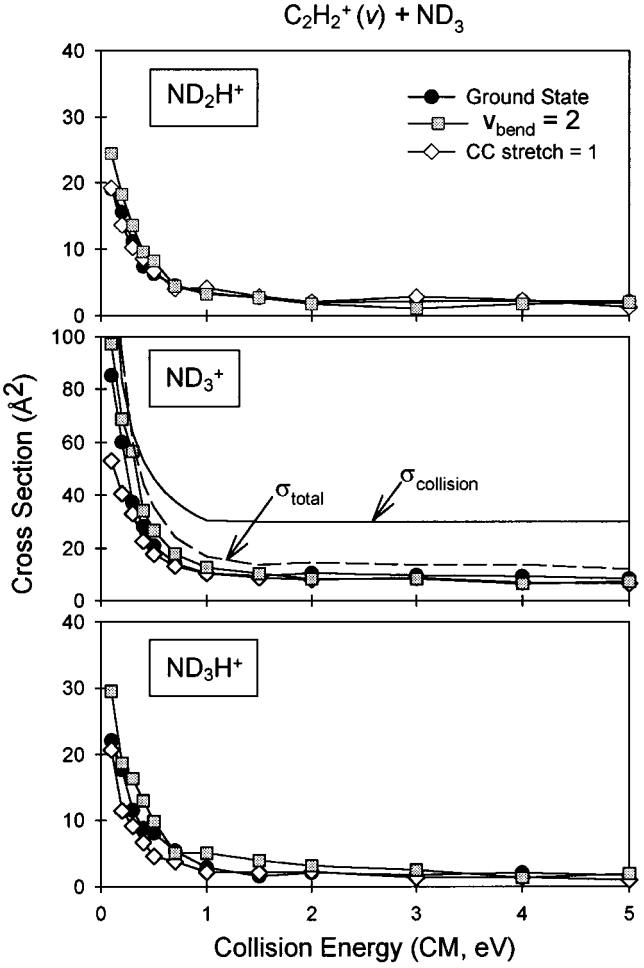

Figure 2. Cross sections for all observed products as a function of collision energy and $C_2H_2^+$ vibrational state.

at low energies and an estimated hard-sphere cross section at high energies ($\sigma_{capture}$ drops below $\sigma_{hardsphere}$ at ~1 eV). At energies below about 0.5 eV, the total cross section is equal to the capture cross section within experimental uncertainty, indicating reaction with unit efficiency. This is consistent with Huntress's thermal rate constant of 3.1×10^{-9} cm^3 s^{-1} and suggests that our collection/detection efficiency is quite good, even though many products are backscattered. By the time collision energy reaches 1 eV, the reaction efficiency is down to ~50%, and it decreases slowly to ~40% at 5 eV.

One ambiguity in the data is that mass 20 may have contributions from both ND_3^+ and $ND_2H_2^+$, i.e., both CT and PT. We can, however, set a reasonable upper limit on how large the $ND_2H_2^+$ contribution might be. If we assume that H and D are completely equivalent in the PT reaction, as might occur in a complex-mediated mechanism, then the ratio of $ND_2H_2^+$ to ND_3H^+ should be about 3:2. In fact, our velocity distribution results (below) show that the PT reaction is better described by a proton-stripping mechanism, and this strongly favors the ND_3H^+ isotopomer. Virtually all PT is direct at high energies, and at least half is direct even at our lowest energy. This suggests that the $ND_2H_2^+$-to-ND_3H^- ratio is ~3:7 at low energies and essentially zero at high energies. This, in conjunction with the observation that the cross section at mass 20 ($ND_3^+ + ND_2H_2^+$) is 3.5−4.5 times larger than σ_{21} (ND_3H^+), suggests that $ND_2H_2^+$ contributes ~15% of the mass 20 signal at our lowest collision energies but is insignificant at higher energies. Except where it matters, we will generally refer to the mass 20 signal as ND_3^+.

It is interesting to note that the CT:PT branching ratio found at our lowest collision energy (0.1 eV) is 80:20, assuming all

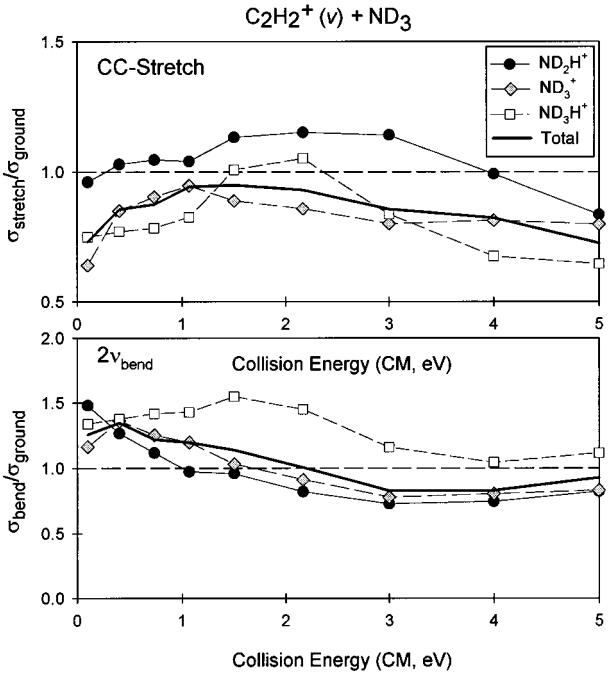

Figure 3. Vibrational effects: $\sigma_{vib}/\sigma_{groundstate}$.

mass 20 is ND_3^+. This compares to a CT:PT ratio of 69:31 found by Huntress under thermal conditions, corresponding to an average collision energy about half our lowest energy. If we take 15% of the mass 20 signal and assign it to PT rather than CT, then the CT:PT ratio is 71:29, i.e., in excellent agreement with Huntress.

Vibrational effects are relatively small in this system but are mode-specific. Figure 3 plots the ratio of the cross sections for $C_2H_2^+$ with CC-stretch or $2\nu_{bend}$ excitation to that for reaction of ground-state $C_2H_2^+$. The solid line is the analogous ratio for the total cross section. Since the product distribution is dominated by ND_3^+, the vibrational effect for σ_{total} followed that for ND_3^+. As the collision energy increases, the vibrational effects become less certain, because the cross sections are much smaller. The structure, such as the fluctuation in the CC-stretch effect on ND_3H^+ between 1.5 and 2.5 eV, is not real, but the larger scale effects are reproducible.

Excitation of the $C_2H_2^+$ CC stretch (1814 $cm^{-1} \approx 225$ meV) inhibits both the ND_3^+ and ND_3H^+ channels by about 25% at low energies. This is ~50% less inhibition than would be gotten by putting the same 225 meV of reactant excitation into collision energy. At higher energies, the effect is smaller—roughly a ~10% inhibition. The ND_2H^+ isotopomer of the CT channel is essentially unaffected by CC stretching.

The effect of $C_2H_2^+$ $2\nu_{bend}$ excitation is larger. All three channels are enhanced by ~30% at low energies. For the two CT products, the enhancement dies off with increasing energy, and there may be a small inhibition above 2 eV. For the PT channel, the enhancement rises to ~60% by 1 eV and then declines slowly with increasing collision energy.

Figure 4 gives representative axial recoil velocity distributions for three different collision energies. Since the vibrational effects on recoil are small, we only plot data for the ground-state reaction. The velocity scale is in the LAB frame, and the dotted vertical line in each frame is V_{CM}. Product ions with velocities higher than V_{CM} are forward scattered in the CM frame (i.e., in the direction of the incident $C_2H_2^+$), while those with lower velocities are backscattered in the CM frame (direction of the incident ND_3 neutral). Defining "forward" as product *ion* recoil in the direction of the reactant ion beam is the usual convention for ion−molecule scattering. It can be a bit

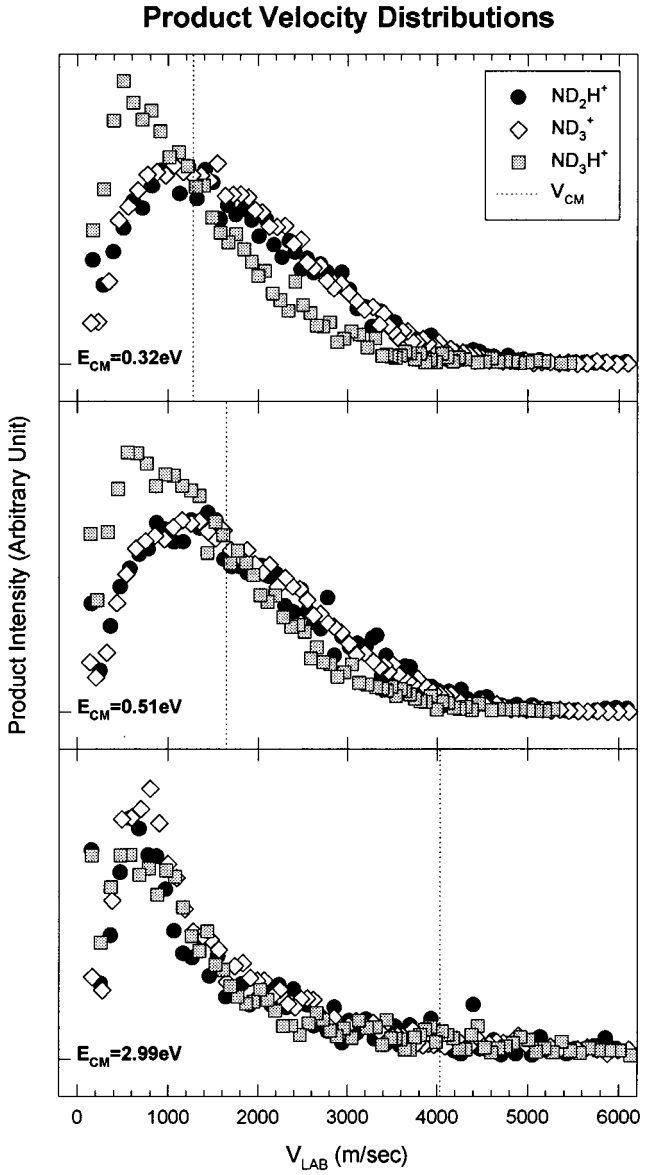

Figure 4. LAB frame axial velocity distributions for three different collision energies. The vertical dashed line indicates the velocity of the center of mass (V_{CM}).

confusing for reactions such as PT and CT where the charge is transferred in the reaction. In this case, rebound scattering is in the *forward* direction, while stripping gives "backward" scattering—i.e., exactly opposite to the usual sense of forward and backward.

For these velocity measurements, the final electrode injecting ions into the octapole guide is kept at a potential below that of the guide. Ions that are backscattered in the LAB frame are, therefore, lost (their velocities can't be measured anyway). In addition, due to the inevitable presence of small potential barriers in the octapoles, ions scattered at low LAB velocities are likely to be lost or have their flight times significantly perturbed. In this case, it is clear that we are losing ions with LAB velocities less than ~750 m/s, corresponding to ions with energies ≤60 meV. In fitting the velocity distributions, we therefore disregard the velocity range below 750 m/s.

Considerable dynamical insight can be gotten simply by inspecting the raw distributions. The two CT isotopomers (ND_3^+ and ND_2H^+) have very similar recoil velocity distributions. At the lowest energy, the distributions are consistent with forward−backward symmetry, and the shapes suggest that there may be a substantial tail of the distribution that is scattered at low or negative LAB velocities and thus lost. This is confirmed

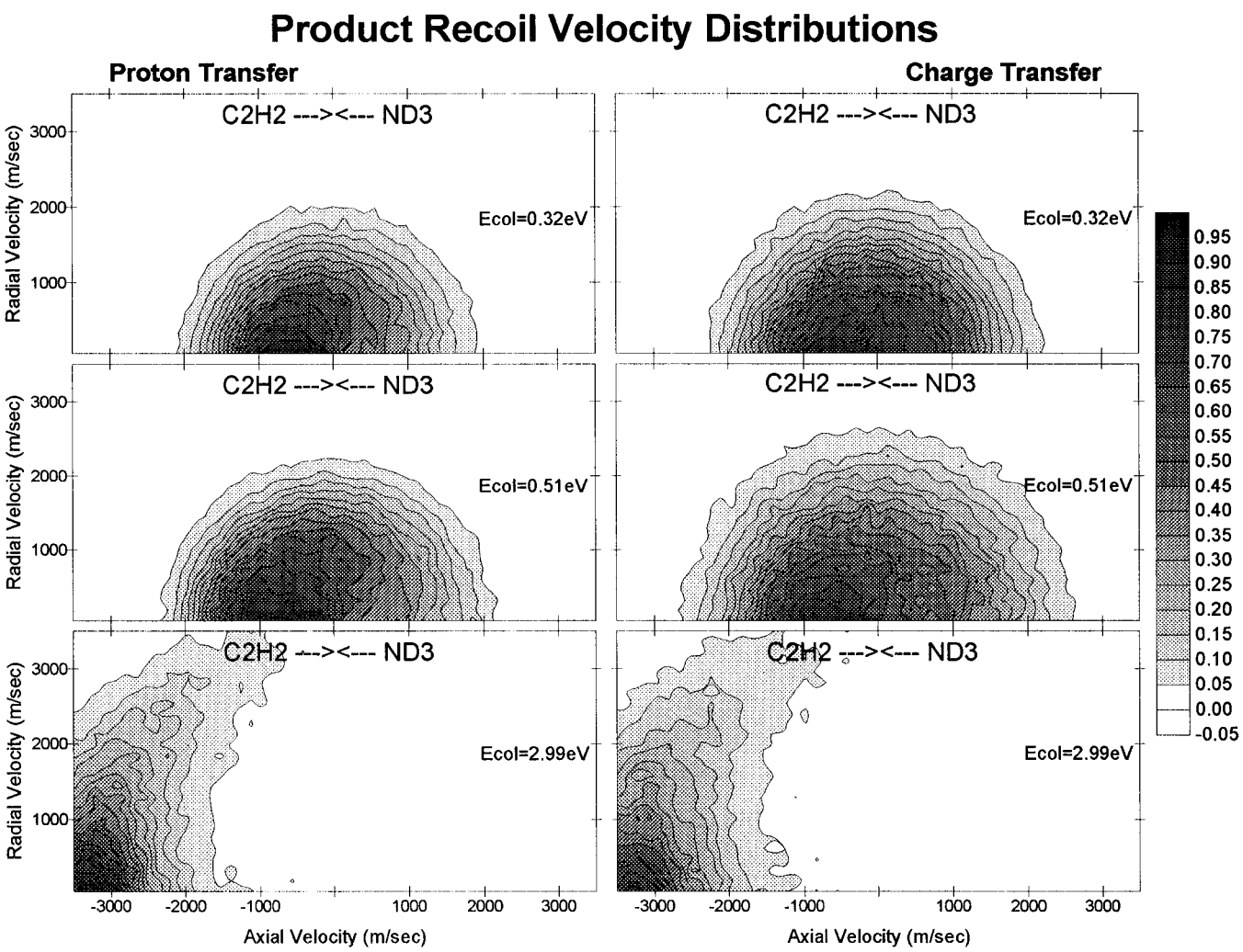

Figure 5. Recoil velocity distribution contour plots resulting from simulations of the data in Figure 4.

by the fact that when the octapole injection lens voltage is raised to reflect the backscattered product ions, there is a substantial increase in the CT signal. As the collision energy is raised, V_{CM} shifts forward in the LAB frame, but the peak of both CT recoil distributions shifts backward. Already by 0.51 eV, there is a small forward−backward asymmetry, and by 3 eV, the distributions are strongly backward-peaked. Particularly at the highest collision energy, it is quite likely that a substantial fraction and possibly even the peaks of the CT recoil distributions are scattered with $v_{LAB} < 750$ m/s.

In contrast, the PT product (ND_3H^+) shows a clar propensity to backscatter at all collision energies. The tendency to backscattering is found even at collision energies as low as 0.1 eV, indicating that the PT reaction goes at least partly by a direct mechanism, even at near-thermal energies.

The recoil distributions have been fit, as discussed above. The best fits are selected visually and lie within the scatter of the data points over the entire velocity range greater than 750 m/s. Contour maps of the resulting velocity distributions are shown in Figure 5, and Table 1 summarizes some of the results. Because the simulations for ND_2H^+ and ND_3^+ are similar, only the latter are plotted. Keep in mind that the fitting is somewhat model dependent and also that we may be missing the strongly backscattered part of the distribution. The tabulated fraction of E_{avail} appearing as recoil should therefore be regarded as a lower limit.

TABLE 1: Simulation Results

product	$\langle E_{col}\rangle^a$	$\langle E_{avail}\rangle$	$\langle E_{recoil}\rangle$	$\Delta(E_{recoil})^b$	$\langle E_{recoil}\rangle/\langle E_{avail}\rangle$
NH_2H^+	0.32	1.60	0.44	0.36	0.28
ND_3^+	0.32	1.60	0.44	0.36	0.28
ND_3H^+	0.32	1.27	0.29	0.24	0.23
ND_2H^+	0.52	1.80	0.50	0.41	0.28
ND_3^+	0.52	1.80	0.50	0.41	0.28
ND_3H^+	0.52	1.46	0.36	0.28	0.25
ND_2H^+	3.0	4.29	2.04	0.90	0.48
ND_3^+	3.0	4.29	2.26	0.88	0.52
ND_3H^+	3.0	3.95	1.97	0.89	0.49

[a] Quantities in angle brackets are mean values. Unit is eV. [b] Width (as standard deviation) of E_{recoil} distribution.

IV. Discussion

A. Missing Channels. The biggest surprise in this reaction is that only CT and PT reactions are observed, despite the existence of many other energetically accessible product channels. Given the many similarities between the $C_2H_2^+/NH_3$ and $C_2H_2^+/CH_4$ systems, it is remarkable that the product distributions are completely orthogonal. For methane, reaction at low energy is dominated by the formation and decomposition of a covalently bound $C_3H_6^+$ complex, while at high energies, a direct H atom abstraction reaction dominates. For ammonia, despite the existence of several strongly bound $C_2H_5N^+$ species (Figure 1), it appears that the system does not explore the covalently bound part of the potential surface at all. This conclusion is based on the consideration that if such a $C_2H_5N^+$ complex formed, it is inconceivable that the H-elimination product channels would not be a major decomposition pathway. Other products (e.g., H_2 elimination) would also likely result from decay of such a complex, but for H elimination, there is no chance that there might be an activation barrier blocking the reaction.[26] Apparently, there is either a substantial barrier

or a severe dynamical bottleneck that prevents the reactants from forming the covalently bound $C_2H_5N^+$ complex at all.

Also not observed is the H atom abstraction reaction producing $C_2H_3^+ + NH_2$. This is especially odd in light of the importance of the analogous, and energetically similar, channel in the $C_2H_2^+/CH_4$ reaction. It seems unlikely that there would be a substantial exit channel barrier for this ion−radical product pair. Furthermore, it is clear that there is no entrance channel barrier since the proton-transfer reaction is highly efficient at low energies. Finally, this reaction in the $C_2H_2^+/CH_4$ system is direct; thus, it seems unlikely that the barrier/bottleneck that prevents $C_2H_5N^+$ complex formation would also prevent H atom abstraction. We are left with the conclusion that there must be a dynamical bottleneck that effectively shuts down H abstraction. One possibility is that the ion−dipole interaction between the approaching $C_2H_2^+$ and ND_3 orients the reactants so that $C_2H_2^+$ always attacks on the nitrogen end of ND_3. This would occur both by locking the ND_3 dipole to the intermolecular axis and also by the fact that the ion approach should lift the degeneracy of the double-well ND_3 bending potential, effectively forcing the D atoms away from the approaching $C_2H_2^+$.

This argument is appealing from an intuitive point of view. Without additional information on the early portions of the $C_2H_2^+$:ND_3 potential and probably some trajectory calculations, it is not clear whether the orienting effect and the resulting steric hindrance would be large enough to explain the complete absence of H atom abstraction. Another possible rationalization might be that the presence of exoergic competing *direct* channels is enough to block the H-abstraction reaction. In the case of $C_2H_2^+/CH_4$, the competing exoergic channels are all complex-mediated, and both our results[5] and Klippenstein's calculations[12] indicated that the complex/direct branching was controlled early on in the collision. For ammonia, the PT and CT reactions are each direct and efficient. The problem with this competition hypothesis is that we would expect a non-zero branching toward H atom abstraction, especially at high collision energies.

B. Proton Transfer. The dynamics for the proton-transfer reaction are clearly revealed by the data. The raw velocity distributions are backward peaked, even at 0.1 eV collision energy, and at high energies, the signal is almost entirely in a sharp backscattered peak. What this tells us is that even at low collision energies, the reaction is direct in the sense that the average collision time is less than ∼300 fs (i.e., about one-third of the ∼1-ps complex rotational period). As the collision energy is increased, the sharply backscattered distribution requires that the time scale of the collision be even shorter. Within the framework of the osculating complex model discussed above, the best fit collision time is ∼5% of $\tau_{complex}$, or about 50 fs.

Strong backward peaking is the signature of a proton-stripping reaction, in which ND_3 captures a proton from $C_2H_2^+$ and then continues on its way with little momentum transfer. In the limit of pure spectator stripping,[27] we would expect the distribution for $E_{col} = 0.32$, 0.51, and 3.0 eV to peak backwards at −1170, −1510, and −3690 m/s, respectively, in the CM frame. In the simulations (Figure 5), the peaks of the distributions do approach these limits as the collision energy is raised. It is hard to say how closely the dynamics approach spectator behavior because these limiting velocities are all at LAB velocities < 750 m/s. Certainly the results are consistent with an approach to spectator behavior.

This reaction is exoergic by 0.95 eV, and it is interesting to see how much of this energy is partitioned into recoil. At a collision energy of 0.32 eV, the total energy available to the products (E_{avail}) is 1.27 eV. The simulations suggest that the average recoil velocity ($\langle E_{recoil} \rangle$) is about 23% of E_{avail}. As the collision energy is increased, the fraction of energy going in to recoil increases as well, to about 50% at 3 eV. Note that because of collection problems with ions scattered at v_{LAB} < 750 m/s, these are lower limits. In any case, it is clear that the fraction going into recoil is far higher than the 5.5% that would be observed with energy equally partitioned to all degrees of freedom. This is all consistent with a direct stripping mechanism.

The PT reaction is about 15−20% efficient at low energies, dropping to ∼5% at high energies. This also seems to be consistent with the proposed mechanism. At higher energies, the direct proton-stripping reaction presumably requires a collision geometry where the nitrogen lone pair collides with one of the $C_2H_2^+$ protons and, further, that the ND_3H^+ product is able to miss colliding with the heavy atoms in the remaining C_2H moiety. Evidently other geometries do not contribute to the high energy PT reaction, and this explains the rather low efficiency. As collision energy is decreased, the reaction is still direct, but the collision time scale increases to several hundred femtoseconds, and this may allow the reactants time to adjust for at least small deviations from the ideal geometry, thus increasing efficiency.

Over our entire energy range, the PT reaction is enhanced by $C_2H_2^+$ bending excitation and inhibited by the CC stretch. A possible explanation for the vibrational effects at low collision energies is given in the next section. The bending enhancement at high collision energies is unique to the PT channel and thus must be due to some influence on the probability of proton stripping. Bending in $C_2H_2^+$ disrupts the sp hybridization to some extent and, thus, may weaken the CH bonds, thus facilitating stripping. On the other hand, this reaction goes at considerably less than unit efficiency, possibly due to the steric effects just mentioned. One could imagine that bending might reduce the interference to some extent. A definitive answer will probably require more information about the stationary states early on the $C_2H_2^+$−NH_3 potential surface.

C. ND_3^+: Change Transfer without H/D Exchange. The dynamics of charge transfer are somewhat different. At energies up to about 0.5 eV, the ND_3^+ recoil velocity distribution is forward−backward symmetric, consistent with the bulk of CT being mediated by a complex with lifetime greater than ∼1 ps. As the collision energy is increased, the recoil velocity distribution shifts backward in the CM frame so that by 3 eV, most of the products are scattered at low LAB velocities. The CT efficiency ($\sigma_{CT}/\sigma_{collision}$) for ground-state $C_2H_2^+$ drops from ∼65% at low energies to ∼35% at 1 eV and then is roughly constant at higher energy.

The strong backscattering at high energies implies a mechanism where the charge is transferred with little momentum transfer, leaving the ND_3^+ product with near zero LAB velocity. This type of mechanism is not unexpected for exoergic charge transfer between polyatomic molecules. The density of product vibrational states gives a reasonably high probability of there being near-resonant CT channels where little energy/momentum transfer is required to conserve energy. This allows CT by electron hopping at long-range curve crossings, giving rise to high-energy CT cross sections that can be quite large—sometime larger than $\sigma_{hardsphere}$. That is the case, for example, in the $C_2H_2^+$/OCS system,[3] while for $C_2H_2^+/ND_3$ the high-energy CT cross section is only approximately one-third $\sigma_{hardsphere}$.

For a truly long-range mechanism, the CT efficiency can be rationalized by a Franck−Condon/energy gap model,[3,28,29] where CT is most probable for states that are near resonant and that also have sizable Franck−Condon overlap with the initial reactant state. This gives a plausible explanation for why the

high-energy CT probability is so low. C_2H_2, when ionized, undergoes only a small expansion of the CC bond length, and the dominant states produced in the ion are the ground state and the first few members of a progression in ν_2.[30] For neutralization, we expect a similar propensity for only a few levels of ν_2 to be Franck−Condon active. For ND_3, the large geometry change accompanying ionization leads to a photoelectron spectrum[17] with a long progression in ν_2, the umbrella bend. If we assume that most of the CT exoergicity has to be taken up as ND_3^+ umbrella motion, then to achieve resonance with the reactant state, excitation to $\nu_2 \approx 13$ would be required. Judging from the photoelectron spectra, the Franck−Condon factor for the ND_3^+ ($\nu_2 = 13$) ← ND_3 ($\nu_2 = 0$) transition is only about 10% of the peak Franck−Condon factor ($\nu_2 = 5-7$). Of course, it is likely that other ND_3^+ or C_2H_2 vibrational states may take up some of the excess energy, but the point is that the aggregate Franck−Condon factors for near-resonant CT are quite poor. CT still takes place primarily at long range, as shown by the strongly backward-peaked velocity distribution, but the probability is relatively low. In this energy regime, both CC stretch and bend excitation inhibit CT by 10−20%, and the effect is larger for the higher energy stretch excitation. This could be a Franck−Condon effect, but it may also be due to larger energy gaps. We are unable to estimate the gaps because the vibrational level spacings are not known at the higher energies required to achieve resonance.

At low collision energies, the much increased CT efficiency, together with the forward−backward symmetric recoil distributions, indicate that a new CT mechanism is dominating. The logical mechanism is CT mediated by a complex with ∼1-ps lifetime. This is clearly not a covalently bound $C_2H_5N^+$ complex, since the H and H_2 elimination products from such a complex are not detected. This must simply be a complex of the $[C_2H_2{:}NH_3]^+$ form, weakly bound by electrostatic forces. The fact that a substantial cross section is observed for the H/D-exchanged CT product (ND_2H^+) is consistent with a complex-mediated mechanism, though clearly this is not a case where the H/D atoms are completely scrambled, since that would lead to a predominance of ND_2H^+ over ND_3^+. Evidently H/D migration is inefficient in this $[C_2H_2{:}NH_3]^+$ complex, probably due to the short lifetime, and this also explains the fact that the complex-mediated mechanism does not lead to much ND_3H^+ PT product.

At low energies, the vibrational effects are quite mode-specific. CC-stretch excitation inhibits CT by ∼25%, and $2\nu_{bend}$ excitation enhances CT by ∼30%. Since the dominant low-energy CT mechanism seems to be complex-mediated, the vibrational effects must originate early in the collision, prior to formation of the $[C_2H_2{:}NH_3]^+$ complex. The reasoning here is that the initially prepared vibrational modes would be scrambled in the complex; thus, the observed and mode specificity requires that the rate-limiting step be prior to complex formation.

In fact, the vibrational effects on all three channels are similar at low energies, and the net effect is that total reactivity is enhanced by $C_2H_2^+$ bending and inhibited by CC stretching. This suggests a reaction mechanism where the $C_2H_2^+$ vibration influences the probability of a successful reactant approach, while the branching between the product channels is determined later in the collision by factors (e.g. geometry or total energy) not strongly dependent on $C_2H_2^+$ vibration. One possibility is that vibration is controlling the probability for transition to the $ND_3^+ + C_2H_2$ charge state, early in the collision, and that ND_3H^+ and ND_2H^+ products, as well as the CT products, form in this charge state. It is not clear what aspect of the $C_2H_2^+$ vibrations enhances or inhibits the likelihood of a reactive collision, and theoretical insight would be very helpful.

D. ND_2H^+ Enigma. The H/D-scrambled CT product, ND_2H^+, is observed to have a collision energy dependence and recoil velocity distributions quite similar to the dominant CT product, ND_3^+. At low collision energies, this is entirely reasonable. CT appears to go via a complex-mediated mechanism, and in this case, we expect to find a fraction of CT products where some H/D scrambling has occurred.

More surprising is that this product is observed at high collision energies, where CT is dominated by long-range electron hopping. There is, however, bound to be some CT occurring in more intimate collisions, and these would allow the necessary H/D exchange. The real puzzle is that the recoil velocity distribution for the ND_2H^+ product is quite similar to that for ND_3^+, even at high energies. It would seem that any collisions intimate enough to allow H/D exchange should also result in significant momentum transfer and, thus, products that are not so strongly backscattered.

We considered the possibility that our ND_3 reactant was somehow undergoing exchange in the inlet system so that there was significant ND_2H contamination. This was checked by electron impact ionizing the ND_3 inside the octapole guide, just at the exit of the scattering cell. The mass spectrum shows no peaks at odd masses, indicating insignificant H contamination. One might also think that ND_2H^+ might arise from decomposition of nascent ND_3H^+ product. The problem with this hypothesis is that the net reaction

$$C_2H_2^+ + ND_3 \rightarrow ND_3H^+ + C_2H \rightarrow ND_2H^+ + H + C_2H$$

is endoergic by 4.5 eV, so this channel is closed over most of our collision energy range.

The data, therefore, indicate that there is some subset of collisions that can exchange an H/D pair along with the charge but without substantial momentum transfer. Actually, there is evidence suggesting that some momentum transfer does take place in the collisions, leading to ND_2H^+. Although the velocity distributions in Figure 4 look identical for ND_3^+ and ND_2H^+, when we raise the potential on the lens injecting ions into the octapole so that backscattered ions are collected, the signal for ND_3^+ increases by ∼30%, while the ND_2H^+ signal is unchanged. This indicates that the ND_2H^+ product is less backscattered than the ND_3^+. Still, the degree of backscattering is quite surprising, and it is really not clear what collision dynamics lead to this.

This two most likely scenarios might be thought of as D transfer followed by H^+ backtransfer:

$$C_2H_2^+ + ND_3 \rightarrow ND_2{:}C_2H_2D^+ \rightarrow ND_2H^+{:}C_2HD \rightarrow ND_2H^+ + C_2HD$$

or H^+ transfer followed by D atom backtransfer:

$$C_2H_2^+ + ND_3 \rightarrow ND_3H^+{:}C_2H \rightarrow ND_2H^+{:}C_2HD \rightarrow ND_2H^+ + C_2HD$$

Both would have to occur in a very short-lived encounter complex to be consistent with the observed strongly peaked recoil distribution. The first seems unlikely, since we might expect that in some collisions the products would separate after the first step, giving rise to a $C_2H_2D^+$ channel that is not observed. The second possibility simply corresponds to proton transfer but where a backtransfer of a D atom occurs before the products can separate. In this mechanism, product separation before backtransfer simply would give the observed PT product channel. We might expect, however, that the ratio of ND_3H^+ to ND_2H^+ would increase with collision energy, since the time

available for the backtransfer is decreased. In fact, this ratio is found to be approximately energy-independent.

V. Conclusions

We have found that the $C_2H_2^+ + NH_3$ system has some very interesting and complex dynamics. The combination of reactant ion state selection and product ion velocity measurements provides a reasonably complete picture of the reaction mechanisms, though some important questions remain. Perhaps most interesting is what feature(s) of the potential surface prevents $C_2H_5N^+$ complex formation and the H atom abstraction reaction. Both of these processes were expected to be important from comparisons with the $C_2H_2^+ + CH_4$ reaction. To further explore this system, we are currently running similar experiments on the $NH_3^+ + C_2H_2$ system, where we can also mode-selectively excite the reactant ion.

Acknowledgment. This work is supported by the Experimental Physical Chemistry program of the National Science Foundation (CHE-950802).

References and Notes

(1) Anderson, S. L. *Adv. Chem. Phys.* **1992**, *82*, 177.
(2) Yang, B.; Chiu, Y.; Anderson, S. L. *J. Chem. Phys.* **1991**, *94*, 6459.
(3) Orlando, T. M.; Yang, B.; Chiu, Y.; Anderson, S. L. *J. Chem. Phys.* **1990**, *92*, 7356.
(4) Chiu, Y.; Fu, H.; Huang, H.; Anderson, S. L. *J. Chem. Phys*. **1994**, *101*, 5410.
(5) Chiu, Y.; Fu, H.; Huang, H.; Anderson, S. L. *J. Chem. Phys*. **1995**, *102*, 1199.
(6) Chiu, Y.; Yang, B.; Fu, H.; Anderson, S. L.; Schweizer, M.; Gerlich, D. *J. Chem. Phys.* **1992**, *96*, 5781.
(7) Yang, B.; Chiu, Y.; Fu, H.; Anderson, S. L. *J. Chem. Phys*. **1991**, *95*, 3275.
(8) Orlando, T. M.; Yang, B.; Anderson, S. L. *J. Chem. Phys*. **1989**, *90*, 1577.
(9) Chiu, Y.; Fu, H.; Huang, J.; Anderson, S. L. *J. Chem. Phys*. **1995**, *102*, 1188.
(10) Chiu, Y.; Fu, H.; Huang, J.; Anderson, S. L. *J. Chem. Phys*. **1996**, *105*, 3089.
(11) Anderson, S. L. *Acc. Chem. Res.* **1997**, *30*, 28.
(12) Klippenstein, S. J. *J. Chem. Phys*. **1996**, *104*, 5437.
(13) Lias, S. G.; Bartmess, J. E.; Liebman, J. F.; Holmes, J. L.; Levin, R. D. *J. Phys. Chem. Ref. Data* **1988**, *17*, suppl. 1.
(14) RRKM lifetime estimates corresponding to the lowest and highest collision energies studied in our experiment.
(15) Lias, S. G.; Liebman, J. F.; Levin, R. D. *J. Phys. Chem. Ref. Data* **1984**, *13*, 695.
(16) Metayer-Zeitoun, C.; Alcarez, C.; Anderson, S. L.; Palm, H.; Dutuit, O. *J. Phys. Chem*. **1995**, *99*, 15523.
(17) Rabalais, J. W. *Principles of Ultraviolet Photoelectron Spectroscopy*; Wiley: New York, 1977.
(18) Huntress, W. T., Jr. *Astrophys. J. Suppl. Ser*. **1977**, *33* (4), 495.
(19) Orlando, T. M.; Anderson, S. L.; Appling, J. R.; White, M. G. *J. Chem. Phys*. **1987**, *87*, 852.
(20) Ashfold, M. N.; Tutcher, B.; Yang, B.; Jin, Z.; Anderson, S. L. *J. Chem. Phys*. **1987**, *87*, 5105.
(21) Ikezoe, Y.; Matsuoka, S.; Takebe, M.; Viggiano, A. *Gas phase ion-molecule reaction rate constants through 1986*; Mass Spec. Soc. of Japan (Distrib. by Maruzen Ltd): Tokyo, 1987.
(22) Adams, N. G.; Smith, D.; Henchman, M. J. *Int. J. Mass Spectrom. Ion Phys.* **1982**, *42*, 11.
(23) Gerlich, D. *Adv. Chem. Phys*. **1992**, *82*, 1.
(24) Fisk, G. A.; McDonald, J. D.; Herschbach, D. R. *Discuss. Faraday Soc*. **1967**, *44*, 228.
(25) Troe, J. *Chem. Phys. Lett*. **1985**, *122*, 425.
(26) That would imply an unprecedented activation barrier for the reverse ion−radical recombination reaction.
(27) Levine, R. D.; Bernstein, R. B. *Molecular Reaction Dynamics and Chemical Reactivity*; Oxford University: New York, 1987.
(28) Houle, F. A.; Anderson, S. L.; Gerlich, D.; Turner, T.; Lee, Y. T. *Chem. Phys. Lett*. **1981**, *82*, 392.
(29) Anderson, S. L.; Turner, T.; Mahan, B. H.; Lee, Y. T. *J. Chem. Phys*. **1982**, *77*, 1842.
(30) Dehmer, P. M.; Dehmer, J. L. *J. Electron Spectrosc. Relat. Phenom*. **1982**, *28*, 145.